AIP | Applied Physics Letters

Strain and vacancy cluster behavior of vanadium and tungsten-doped Ba[Zr0.10Ti0.90]O3 ceramics

F. Moura, A. Z. Simões, L. S. Cavalcante, M. Zampieri, J. A. Varela et al.

Citation: Appl. Phys. Lett. **92**, 032905 (2008); doi: 10.1063/1.2837196
View online: http://dx.doi.org/10.1063/1.2837196
View Table of Contents: http://apl.aip.org/resource/1/APPLAB/v92/i3
Published by the AIP Publishing LLC.

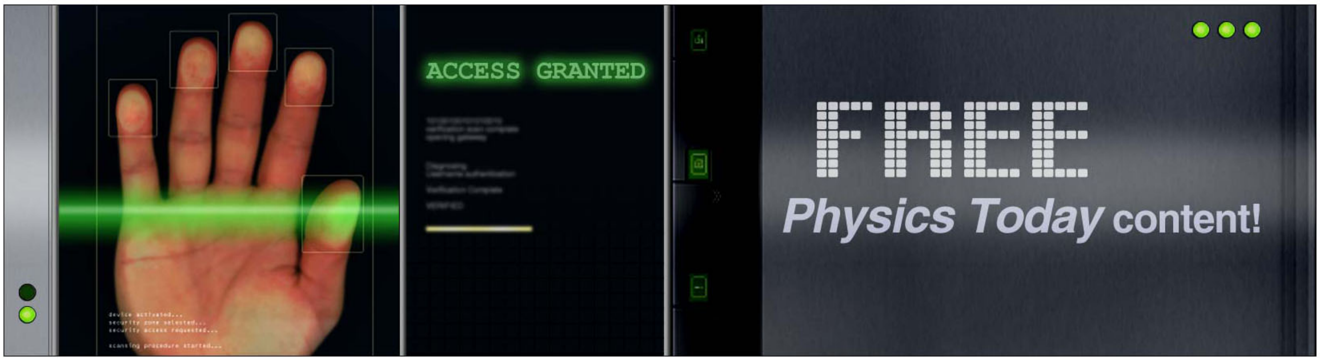

APPLIED PHYSICS LETTERS **92**, 032905 (2008)

Strain and vacancy cluster behavior of vanadium and tungsten-doped $Ba[Zr_{0.10}Ti_{0.90}]O_3$ ceramics

F. Moura, A. Z. Simões, L. S. Cavalcante,[a] M. Zampieri, J. A. Varela, E. Longo, and M. A. Zaghete
Instituto de Química, UNESP, P.O. Box 355, 14801-907 Araraquara, São Paulo, Brazil
and Departamento de Química, UFSCar, P.O. Box 676, São Carlos, 13565-905 São Paulo, Brazil

M. L. Simões
EMBRAPA Agricultural Instrumentation, P.O. Box 741, São Carlos, 13560-970 São Paulo, Brazil

(Received 8 October 2007; accepted 1 January 2008; published online 25 January 2008)

Strain and vacancy clusters behavior of polycrystalline vanadium (V) and tungsten (W)-doped $Ba[Zr_{0.10}Ti_{0.90}]O_3$, (BZT:2%V) and (BZT:2%W) ceramics obtained by the mixed oxide method was evaluated. Substitution of V and W reduces the distortion of octahedral clusters, decreasing the Raman modes. Electron paramagnetic resonance data indicate that the addition of dopants leads to defects and symmetry changes in the BZT lattice. Remnant polarization and coercive field are affected by V and W substitution due the electron-relaxation mode. The unipolar strain *E* curves as a function of electric field reach its maximum value for BZT:2%V and BZT:2%W ceramics. © *2008 American Institute of Physics*. [DOI: 10.1063/1.2837196]

Very high piezoelectric and electrostrictive properties have been achieved in a series of lead based perovskite-type relaxor ferroelectric single crystals[1,2] for a certain orientation. It is believed that in these systems, the high strain is engendered by phase switching from low to high spontaneously deformed states and that the usual hysteresis in such a process is moderated by an induced monoclinicity, which permits almost continuous rotation of the polarization vector. Unfortunately, lead compounds are toxic so there is an increasing desire to develop lead-free materials with high strain capability.[3] Among several groups of lead-free candidates, $BaTiO_3$ (BTO) is known to have a large electromechanical coupling factor. Substitution of Ti^{4+} by Zr^{4+} exhibits several interesting features in the dielectric behavior of BTO ceramics. The effect of doping on various physical and chemical properties of this material is known and this effect has been extensively exploited in piezoelectrics and ferroelectrics to improve their performance. Many aliovalent compositional alterations to $Ba[Zr_xTi_{1-x}]O_3$ have been studied either with higher valence substitutions (donors) or with lower valence ions (acceptors). Donor dopants, such as V^{5+} and W^{6+}, induce cationic defects while occupying the *B* site of the perovskite lattice.[4,5] Such behavior may cause several effects on the dielectric behavior through interaction with domain walls.[6,7] Recently, it was found that in sintering of Y_2O_3-doped BTO with Y_2O_3 higher than 0.80 mol %, presumably exceeded the solid solubility of Y_2O_3 in BTO, is improved by both enhanced densification (by solid-solution defect) and suppressed coarsening (by second-phase pinning).[8] These results demonstrate the performance of our capacitors for future piezoelectric resonators consuming low energy levels at low phase transition temperature. $Ba[Zr_{0.10}Ti_{0.90}]O_3$ (BZT) ceramics were prepared by solid-state reaction. $BaCO_3$, TiO_2, and ZrO_2 starting materials with high purity were weighed and wet mixed in alcohol. After drying, the powders were calcined at 600 °C for 4 h. An aqueous solution of tungsten and vanadium was added to BZT powders. BZT, BZT:2%V, and BZT:2%W were sintered at 1550, 1350, and 1200 °C, respectively, with pellets in a size of about 10×1 mm^2. The density of the sintered compacts was measured by Archimedes method. After sintering, the disks were polished to 1 mm in thickness and characterized by means of electrical measurements. Gold electrodes were applied by evaporation through a sputtering system in a polished surface of sintered discs. Fourier transform Raman (FT-Raman) spectroscopy was performed on Bruker-RFS 100, Germany. A 1064 nm Nd:YAG (yttrium aluminum garnet) laser was used to obtain the Raman spectra as excitation source with its power kept at 85 mW. Ferroelectric properties were measured on a Radiant Technology RT6600A tester equipped with a micrometer probe station in a virtual ground mode. The strain as a function of electric field was measured at 0.2 Hz by a modified Sawyer–Tower circuit and a linear variable displacement. Electron paramagnetic resonance (EPR) spectra were recorded on a Bruker EMX-300 Spectrometer, operating at *X* band (9 GHz) and operating at microwave power of 2 mW, amplitude modulation of 1 G, time constant of 2.56 ms, conversion time of 10.24 ms, and modulation frequency of 100 kHz. The *g* factor was referenced with respect to $MgO:Cr^{3+}$ ($g=1.9797$) as the external standard. All EPR measurements were performed under room temperature (25 °C) and the spectra were evaluated using the SIMFONIA program.

Evolution of Raman spectra in the vanadium and tungsten doped ceramics shows the order-disorder degree of the atomic structure at short range (Fig. 1).

The modes further split into longitudinal (LO) and transverse (TO) components due the long electrostatic forces associated with lattice ionicity caused by Ba^{2+} ions in BTO such as reported in the BZT lattice.[9,10] The spectrum shows the stretching mode of $A_1(TO_1)$ and $A_1(TO_3)$ at around 193 and 517 cm^{-1}, according to the Refs. 11 and 12. The $E_1(TO_1)$ and $E_1(TO_2)$ modes that have been associated with the tetragonal-cubic phase transition[13] were observed at 116 and 301 cm^{-1}, whereas the $A_1(LO_3)$ mode was found at 720 cm^{-1}, with zirconium (Zr) substituting on titanium (Ti)

---

[a] Electronic mail: laeciosc@bol.com.br.

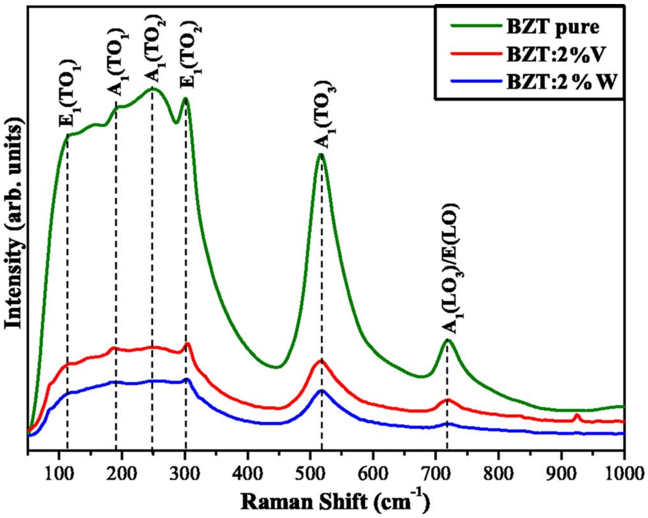

FIG. 1. (Color online) Room temperature depolarized Raman spectra for (a) BZT pure, (b) BZT:2%W, and (c) BZT:2%V ceramics. The vertical dashed lines indicate the position and relative intensity of Raman modes.

sites. However, the coupling between the sharp $A_1(\mathrm{TO}_1)$ and broad $A_1(\mathrm{TO}_2)$ modes reduces as the intensity of $A_1(\mathrm{TO}_2)$ mode decreases.[14,15] As vanadium and tungsten are incorporated in the BZT lattice, a Raman mode at 915 cm^{-1} appears, which reduces the distortion of octahedral clusters, decreasing the relative intensity of bands.

Room-temperature EPR spectrum is shown in Fig. 2.

The reported parameters of the EPR Hamiltonian were used to perfectly reproduce the observed sequence of the symmetrical peak pattern of the fine structure. V and W substitution in the Ti site cause distortion in the lattice being responsible for changes in the spectra. Charges were quantatively measured (spins/g) and are showed in Fig. 2. The observed signal is typical of oxygen vacancies, as cited in the Ref. 16. BZT:2%W also shows hyperfine bands which are typical of materials with paramagnetic ion . That can be attributed to the paramagnetic W^{5+} $(5d^1)$ ions, according to the Ref. 17, supporting the high symmetry as inferred from Raman studies. Moreover, it suggests the almost isotropic neighborhood of the isolated Zr and Ti ions in the pattern.

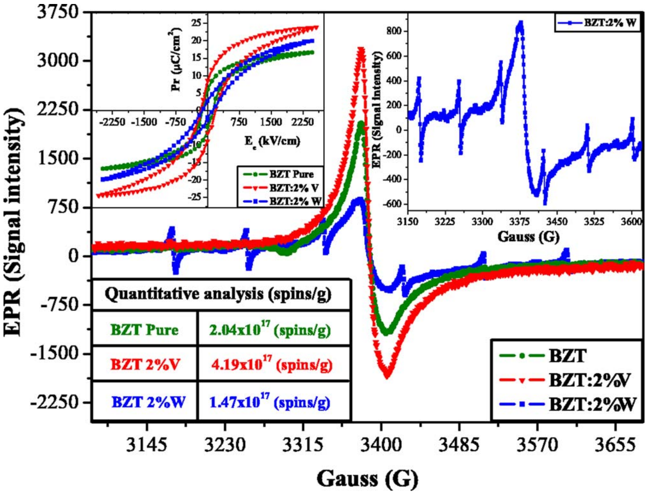

Quantitative analysis (spins/g)	
BZT Pure	2.04x10^{17} (spins/g)
BZT 2%V	4.19x10^{17} (spins/g)
BZT 2%W	1.47x10^{17} (spins/g)

FIG. 2. (Color online) Electron paramagnetic resonance measurements for BZT pure, BZT:2%W, and BZT:2%V ceramics. The inset shows the *P-E* hysteresis loops for BZT pure, BZT:2%W, and BZT:2%V ceramics and quantitative analysis of EPR.

There is an increase in the defects and symmetry changes in the BZT lattice as vanadium and tungsten are added in the system. The main difference in the spectra corresponds to the expected line broadening attributed to dipolar interactions of vanadium and tungsten in the host, according to Eqs. (1)–(13):

$$WO_3 \xrightarrow{\mathrm{BZT}} W^{\cdot}_{\mathrm{Ti}} + V''_{\mathrm{Ba}} + 3\mathrm{O}^x_{\mathrm{O}}, \tag{1}$$

$$[M\mathrm{O}_6]^x_c + [M\mathrm{O}_5 \cdot V^x_{\mathrm{O}}]^x_c \rightarrow [M\mathrm{O}_6]'_c + [M\mathrm{O}_5 \cdot V^{\bullet}_{\mathrm{O}}]_c, \tag{2}$$

where M=Zr or Ti and c=complex;

$$[V''_{\mathrm{Ba}}\mathrm{O}_{12}]_c + [W\mathrm{O}_6]''_c \rightarrow [V^x_{\mathrm{Ba}}\mathrm{O}_{12}]_c + [W\mathrm{O}_6]^x_c, \tag{3}$$

$$[M\mathrm{O}_5 \cdot V^x_{\mathrm{O}}]_c + [W\mathrm{O}_6]''_c \rightarrow [M\mathrm{O}_5 \cdot V^{\bullet}_{\mathrm{O}}]_c + [W\mathrm{O}_6]'_c, \tag{4}$$

$$[M\mathrm{O}_5 \cdot V^x_{\mathrm{O}}]_c + [W\mathrm{O}_6]'_c \rightarrow [M\mathrm{O}_5 \cdot V^{\bullet}_{\mathrm{O}}]_c + [W\mathrm{O}_6]^x_c, \tag{5}$$

$$2[M\mathrm{O}_6]'_c + [W\mathrm{O}_6]''_c \rightarrow 2[M\mathrm{O}_6]^x_c + [W\mathrm{O}_6]^x_c, \tag{6}$$

$$\mathrm{V}_2\mathrm{O}_5 \xrightarrow{\mathrm{BZT}} 2V_{\mathrm{Ti}} + V''_{\mathrm{Ba}} + 5\mathrm{O}^x_{\mathrm{O}}, \tag{7}$$

$$[M\mathrm{O}_6]^x_c + [M\mathrm{O}_5 \cdot V^x_{\mathrm{O}}]_c \rightarrow [M\mathrm{O}_6]'_c + [M\mathrm{O}_5 \cdot V^{\bullet}_{\mathrm{O}}]_c, \tag{8}$$

$$[V''_{\mathrm{Ba}}\mathrm{O}_{12}]_c + 2[\mathrm{VO}_6]'_c \rightarrow [V^x_{\mathrm{Ba}}\mathrm{O}_{12}]_c + 2[\mathrm{VO}_6]^x_c, \tag{9}$$

$$[M\mathrm{O}_5 \cdot V^x_{\mathrm{O}}]_c + [\mathrm{VO}_6]'_c \rightarrow [M\mathrm{O}_5 \cdot V^{\bullet}_{\mathrm{O}}]_c + [\mathrm{VO}_6]^x_c, \tag{10}$$

$$[M\mathrm{O}_6]'_c + [\mathrm{VO}_6]'_c \rightarrow [M\mathrm{O}_6]'_c + [\mathrm{VO}_6]^x_c, \tag{11}$$

despolarization of $[M\mathrm{O}_5 \cdot V^{\cdot}_{\mathrm{O}}]c$ cluster,

$$[M\mathrm{O}_5 \cdot V^{\bullet}_{\mathrm{O}}]_c + \mathrm{O}_2 \rightarrow [M\mathrm{O}_5 \cdot V^{\bullet}_{\mathrm{O}}] \,.\, \mathrm{O}_{2(ads)}, \tag{12}$$

$$[M\mathrm{O}_5 \cdot V^{\bullet}_{\mathrm{O}}] \cdot \mathrm{O}_{2(ads)} \rightarrow [M\mathrm{O}_5 \cdot V^{\bullet\bullet}_{\mathrm{O}}] \cdot \mathrm{O}'_2. \tag{13}$$

High $[V^{\cdot}_{\mathrm{O}}]$ concentration adsorbs O_2 leading to $[M\mathrm{O}_5 \cdot V^{\cdot\cdot}_{\mathrm{O}}]$ O'_2. This species favors the creation of oxygen vacancies in $[\mathrm{TiO}_6]$ or $[\mathrm{ZrO}_6]$ sites being most of that considered as complex vacancies in BZT lattice. As a consequence, the oxygen vacancy-acceptor ion dipole may interact with polarization within a domain making it movement more difficult to switch.

The inset of Fig. 2 illustrates the hysteresis loops of BZT, BZT:2%V, and BZT:2%W ceramics. All loops are characteristic for materials employed in ferroelectric memories.[18] For BZT:2%V, the remnant polarization increased from 6 to 8.6 μC/cm^2 compared to BZT and decreases after to 2.2 μC/cm^2 for BZT:2%W. The values of dielectric constant at 10 kHz were of 11.660, 6.420, and 15.111 for BZT, BZT:2%W, and BZT:2%V, respectively. Addition of vanadium leads to oxygen vacancies which decrease the stress within the domains,[19] resulting in an increase of coercive field (E_c) from 1.2 to 1.7 kV/cm. The remnant polarization is reduced for BZT:2%W due the electron-relaxation-mode coupling mechanism in which carriers (or polarons, protons, and so on) are coupled with the existing dielectric modes. Besides that, tungsten acts by repulsion with their next nearest neighbors and as a consequence, increases the defects of oxygen octahedral at short range. In this case, the coercive field is unchanged compared to BZT.

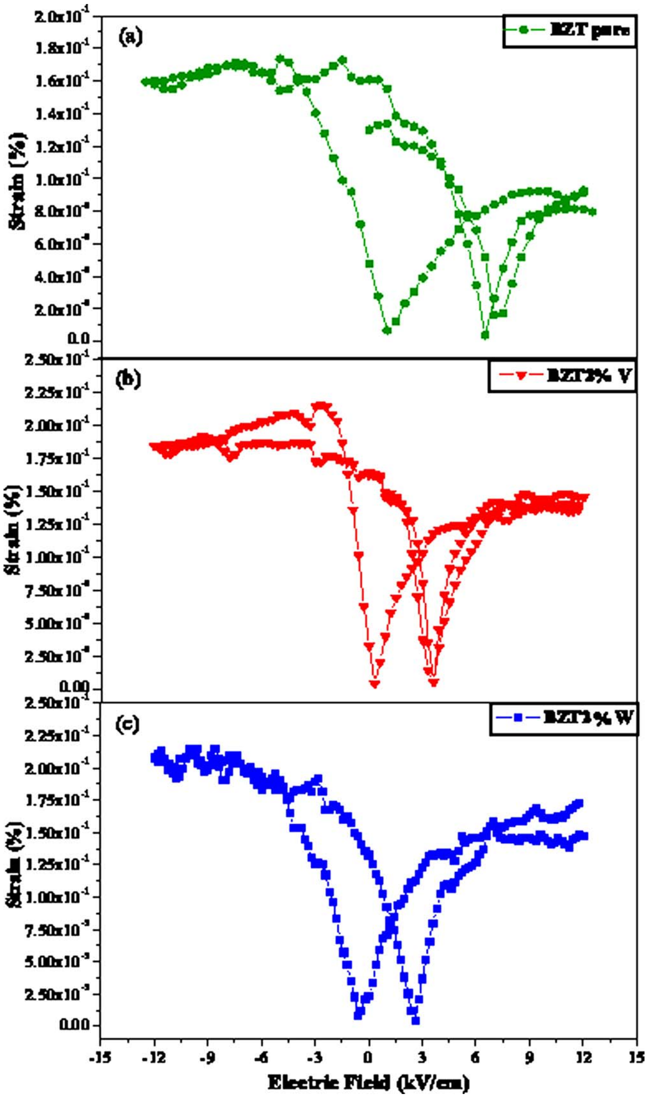

FIG. 3. (Color online) Strain hysteresis as a function of electric field for (a) BZT, (b) BZT:2%W, and (c) BZT:2%V ceramics.

The unipolar strain behavior at room temperature is shown in Fig. 3.

The unipolar strain became a maximum at 5 kV/cm, but saturates at 10 kV/cm. The modifiers increase the strain behavior, in part, due to domain reorientation. Beyond that point, it is possible that a modest bias field results in the transition from asymmetric to symmetric phase. This field-induced phase transition may be ascribed to the pinching effect, that is, the consequent decrease in free energy difference among polymorphic phases. A careful inspection of the *S*-*E* plots reveals that there are two apparent linear regions at low fields ($E < 5$ kV/cm) and high fields ($E > 10$ kV/cm) and one transition region. That corresponds to domain reorientation induced by external electric fields. The hysteretic strain could be associated with domain reorientation. At electric fields higher than 10 kV/cm, the strain is hysteresis free, indicating a stable single domain/poling state induced by the high external electric fields. In addition, from the *S* versus *E* profiles, no noticeable induced phase transition is observed at such high electric fields. It is shown that BZT:2%V and BZT:2%W ceramics exhibit a slightly higher unipolar strain than that for nominally pure BTO ceramics, as shown in Fig. 3. Compared to BZT ($S=0.11\%$), the strain was ($S=0.16$ and 0.19%, respectively) for BZT:2%V and BZT:2%W ceramics, respectively. This is a generally observed phenomenon in doped electronic ceramics, which might be attributed to the improved ceramic quality due to a small amount of impurity doping.

As conclusion, we have shown that the main effect of $[MO_5 \cdot V_O^{\cdot}]\,O_2'$ vacancies in BZT:2%V and BZT:2%W ceramics prepared by the mixture oxide method is the introduction of complex vacancies defects, oxygen vacancies and despolarization of $[MO_5 \cdot V_O^{\cdot}]c$ clusters. As consequence, occurs an increases in the disorder of $[MO_6]$ octahedral at short range (M=Zr or Ti). The unipolar strain behavior was approximately at 5 kV/cm, but decreases and, subsequently, saturates at 10 kV/cm. Raman modes are affected by V and W substitution due the distortion reduction of octahedral clusters. EPR data evidenced disorder and symmetry changes in the BZT lattice while hysteresis data confirm that the substitution is due to the electron relaxation mode in which carriers (polarons, protons, and so on) are coupled with existing dielectric modes.

The authors acknowledge CAPES, FAPESP, and CNPq.

[1] S. E. Park and T. R. Shrout, Mater. Res. Innovations **1**, 20 (1997).
[2] S. E. Park and T. R. Shrout, J. Appl. Phys. **82**, 1804 (1997).
[3] A. Simon, J. Ravez, and M. Maglione, J. Phys.: Condens. Matter **16**, 963 (2004).
[4] Y. Zhi, A. Chen, J. Zhi, P. M. Vilarinho, and J. L. Baptista, J. Appl. Phys. **88**, 410 (2000).
[5] A. Carg and T. C. Goel, Mater. Sci. Eng., B **60**, 128 (1999).
[6] R. Shannigrahi, R. N. P. Choudhary, and N. Acharya, Mater. Sci. Eng., B **56**, 31 (1999).
[7] D. Bolten, U. Bouger, T. Schneller, M. Grossnam, O. Lose, and R. Waser, Appl. Phys. Lett. **77**, 3830 (2000).
[8] H. Y. Lu and M. H. Lin, Ceram. Int. **31**, 989 (2005).
[9] A. Dixit, S. B. Majumder, P. S. Dobal, R. S. Katiyar, and A. S. Bhalla, Thin Solid Films **447**, 284 (2004).
[10] P. S. Dobal and R. S. Katiyar, J. Raman Spectrosc. **33**, 405 (2002).
[11] P. S. Dobal, A. Dixit, R. S. Katiyar, Z. Yu, R. Guo, and A. S. Bhalla, J. Appl. Phys. **89**, 8085 (2001).
[12] J. Kreisel, P. Bouvier, M. Maglione, B. Dkhil, and A. Simon, Phys. Rev. B **69**, 092104 (2004).
[13] B. D. Begg, K. S. Finnie, and E. R. Vance, J. Am. Ceram. Soc. **79**, 2666 (1996).
[14] P. S. Dobal, A. Dixit, R. S. Katiyar, Z. Yu, R. Guo, and A. S. Bhalla, J. Raman Spectrosc. **32**, 69 (2001).
[15] A. Dixit, S. B. Majumder, P. S. Dobal, R. S. Katiyar, and A. S. Bhalla, Thin Solid Films **447**, 284 (2004).
[16] M. Zhang, Z. Jin, J. Zhang, X. Gou, J. Yang, W. Li, X. Wang, and Z. Zhang, J. Mol. Catal. A: Chem. **217**, 203 (2004).
[17] V. V. Laguta, M. Martini, A. Vedda, E. Rosetta, M. Nikl, E. Mihóková, J. Rosa, Y. Usuki, Phys. Rev. B **67**, 205102 (2003).
[18] G. D. Hu, X. Cheng, W. B. Wu, and C. H. Yang, Appl. Phys. Lett. **91**, 232909 (2007).
[19] J. Zhu, X. B. Chen, J. H. He, and J. C. Shen, Phys. Lett. A **362**, 471 (2007).